JOURNAL OF CATALYSIS 118, 125–146 (1989)

Non-Faradaic Electrochemical Modification of Catalytic Activity

1. The Case of Ethylene Oxidation on Pt

S. BEBELIS AND C. G. VAYENAS[1]

Institute of Chemical Engineering and High Temperature Chemical Processes, Department of Chemical Engineering, University of Patras, Patras 26110, Greece

Received June 22, 1988; revised November 22, 1988

It was found that the catalytic activity of polycrystalline Pt for the oxidation of ethylene to CO_2 and H_2O can be increased by up to a factor of 50 when oxygen anions O^{2-} are electrochemically pumped onto the Pt catalyst surface. The experiments were conducted using a stabilized zirconia solid electrolyte at temperatures of 550 to 725 K. The steady-state increase in the catalytic reaction rate is typically 10^5 higher than the rate of O^{2-} transport to the catalyst surface. Over a wide range of conditions the catalytic reaction rate increases exponentially with the catalyst–solid electrolyte overpotential η which is proportional to the change in catalyst work function. The reaction activation energy decreases toward zero with increasing η. The phenomena are completely reversible and show that catalyst work function and catalytic activity can be varied at will by adjusting the catalyst potential. A model which takes into account the change in catalyst work function with changing catalyst activation overpotential and the consequent changes in the bonding strength of chemisorbed species is proposed. The model is in semiquantitative agreement with experiment.

INTRODUCTION

Controlled modification of the electronic and concomitant catalytic properties of metal catalysts has been a long-sought goal in heterogeneous catalysis. The catalytic activity and selectivity of metals can be frequently influenced in desired directions by alloying (*1–3*), by metal–support interactions (*4, 5*), which frequently involve doping of the support (*6*), or by the use of gas phase promoters. Although geometric considerations are often found to play an important role, it is usually accepted that the promoting action of dopants results from changes in the electronic properties of the catalyst, e.g., changes in work function which affect the strength of chemisorptive bonds and, therefore, catalytic activity.

In recent years there has been increasing evidence that the catalytic properties of metal catalysts used as electrodes in solid electrolyte cells can be markedly affected by the use of simple electrochemical techniques. This area has been reviewed recently (*7*). The first application of solid electrolyte cells to study catalytic phenomena involved passive potentiometric measurements of the activity of oxygen on porous metal catalyst films. This technique, usually called solid electrolyte potentiometry (SEP) has been used in conjunction with kinetic measurements to study a number of catalytic reactions on metals (*8–11*). It is particularly suitable for the study of oscillatory reactions (*12–14*).

The same type of solid electrolyte cells with appropriate anodic electrocatalysts can be operated as fuel cells for chemical cogeneration, i.e., for the simultaneous generation of electrical power and chemicals, such as NO from NH_3 (*15–17*), styrene from ethylbenzene (*18, 19*), HCN from CH_4 and NH_3 (*20*), SO_2 from H_2S (*21*), and formaldehyde from methanol (*22*).

The most interesting application of solid

[1] To whom correspondence should be addressed.

0021-9517/89 $3.00

electrolyte cells from the viewpoint of heterogeneous catalysis is their active, or "oxygen pump," mode of operation, where external voltages are applied to cells of the type

gaseous reactants, metal catalyst

$$|ZrO_2\ (8\ \text{mole\%}\ Y_2O_3)|M,\ O_2 \quad (1)$$

and oxygen anions O^{2-} are pumped to or from the catalyst surface. The metal M catalyzes the reaction

$$O_2(g) + 4e^- \leftrightharpoons 2O^{2-} \quad (2)$$

and serves as a means of supplying or removing O^{2-} to or from the porous metal catalyst film through the gas-impervious stabilized zirconia solid electrolyte.

Cells of this type were found to significantly enhance the rate of NO decomposition on Pt and Au (*23, 24*) and the rate of CO hydrogenation on transition metals (*25, 26*).

In these cases the observed rate enhancement was purely Faradaic, in the sense that the increase in the rate of NO decomposition was found equal to the rate of O^{2-} removal from the catalyst. Consequently in this case the enhancement factor Λ defined from

$$\Lambda = \Delta r/(I/2F), \quad (3)$$

where Δr is the change in the catalytic reaction rate (in g-at. O/s) and $(I/2F)$ is the rate of O^{2-} transport through the electrolyte, equals unity. Throughout this paper as in previous papers (*7, 30, 37*) we have defined Δr to be positive when oxygen is consumed in the catalytic reaction and the current I to be positive when it corresponds to O^{2-} being pumped *to* the catalyst. In the case of CO hydrogenation on transition metals (*25, 26*) the published data do not permit an accurate calculation of Λ.

The first report of a non-Faradaic enhancement in catalytic rate, i.e., $\Lambda \gg 1$, was for the case of ethylene and propylene epoxidation and deep oxidation on Ag (*27–29*). It was found that selectivity to the corresponding epoxides increases with positive currents and decreases with negative ones. Values of Λ near 300 were measured. It was proposed that an active oxide layer is formed on the Ag surface due to O^{2-} pumping (*27, 28*). It should be emphasized that the term non-Faradaic simply implies that the change in the *catalytic* reaction rate exceeds the rate of O^{2-} transport which, of course, always equals the *electrocatalytic* rate of reaction (2).

More recently it was found that the rate of CO oxidation on Pt can be markedly affected by O^{2-} pumping (*30*). Enhancement factors Λ on the order of 500 were measured and rate oscillations were found to be induced or stopped at will by adjusting the rate of O^{2-} transport to the catalyst. No quantitative explanation was proposed but it was suggested that O^{2-} pumping must cause changes in the catalyst work function.

In this paper we describe and discuss the effect of O^{2-} pumping on the rate of the Pt catalyzed ethylene oxidation to CO_2 and H_2O, a reaction which has been the subject of several recent investigations (*31–34*). The kinetics and mechanism of this reaction, which under certain conditions exhibits self-sustained oscillations (*12, 32, 35*), have been studied extensively in the past using SEP and simultaneous kinetic measurements without O^{2-} pumping (*12, 35*). Oxygen pumping is found to have a very dramatic effect on this reaction. Rate increases on the order of 5000% and Λ values on the order of 3×10^5 were obtained on the fuel-lean side. However, the major finding of the present work is that the central parameter for understanding this dramatic non-Faradaic electrochemical modification of catalytic activity (for which we propose the acronym NEMCA) is not the current of O^{2-} to the catalyst and therefore Λ, but rather the catalyst–solid electrolyte activation overpotential η, which was accurately measured and which is shown to be proportional to the change in catalyst work function $e\Delta\Phi$. On the basis of this observation it becomes possible to interpret the ob-

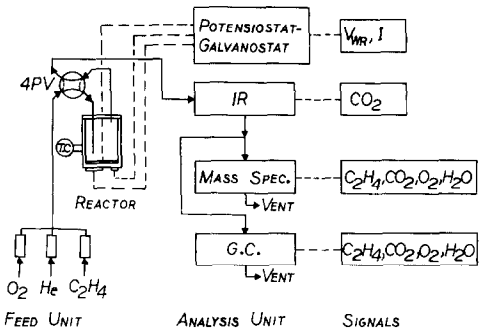

FIG. 1. Schematic diagram of the apparatus.

served dramatic reaction rate increases in a semiquantitative manner. It also becomes possible to accurately predict the magnitude of the enhancement factor Λ not only for this reaction but also for previous studies (*18, 27, 29*).

This paper, which describes the NEMCA effect for the Pt-catalyzed ethylene oxidation, is the first in a series describing similar studies on several other catalytic reactions, such as the CH_3OH dehydrogenation and decomposition on Ag and on Pt (*36, 37*), the methanol oxidation on Pt (*38*), and the partial oxidation of ethylene (*39*) and methane (*40*). We have found no reaction yet for which the NEMCA effect is not operative in the presence of significant (i.e., a few hundred mV) activation overpotential η. It would appear therefore that the NEMCA effect may be of general interest in heterogeneous catalysis.

EXPERIMENTAL

Reactants and Analysis System

The experimental apparatus shown in Fig. 1 has been described in previous papers (*14, 30*). Reactants were Messer Griesheim certified standards of C_2H_4 in He and O_2 in He. They could be further diluted in ultrapure (99.999%) He.

Reactants and products were analyzed by three independent techniques:

(a) On-line gas chromatography using a Perkin–Elmer Sigma 300 gas chromatograph with a TC detector and Perkin–Elmer LCI-100 computing integrator. A Porapak N column was used to separate oxygen, ethylene, CO_2, and H_2O. No other products were detected.

(b) On-line mass spectrometry using a Balzers QMG 311 quadrupole mass spectrometer with a continuous sampling system and a QDP 101 data processor which allowed continuous monitoring of the exit concentrations of O_2, C_2H_4, CO_2, and H_2O.

(c) On-line IR spectroscopy using a Beckman 864 IR CO_2 analyzer, which gave a higher sensitivity to the effluent CO_2 signal than the mass spectrometer, due to the unavoidable vacuum system background noise at AMU 44.

Reactor and Catalyst

The atmospheric pressure stabilized zirconia continuous-flow reactor shown in Fig. 2 has a volume of 30 cm^3 and has been described in detail previously (*12, 14, 30*). All results reported here were obtained at a total volumetric flow rate of 100 cm^3 STP/min. In this flow rate range the reactor has been shown to behave like a CSTR by measuring its residence time distribution using the IR CO_2 analyzer (*12*).

The porous Pt catalyst film was deposited on the inside bottom of the stabilized zirconia tube as described previously (*14, 30*), i.e., by using a thin coating of Engelhard A1121 Pt paste followed by drying and

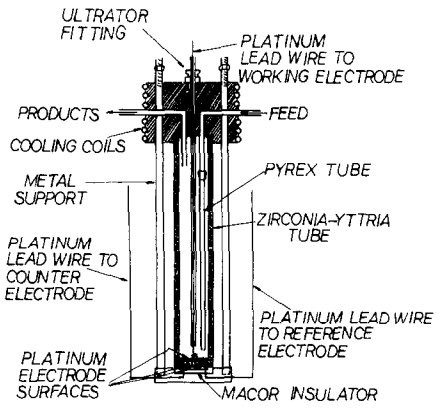

FIG. 2. Reactor configuration.

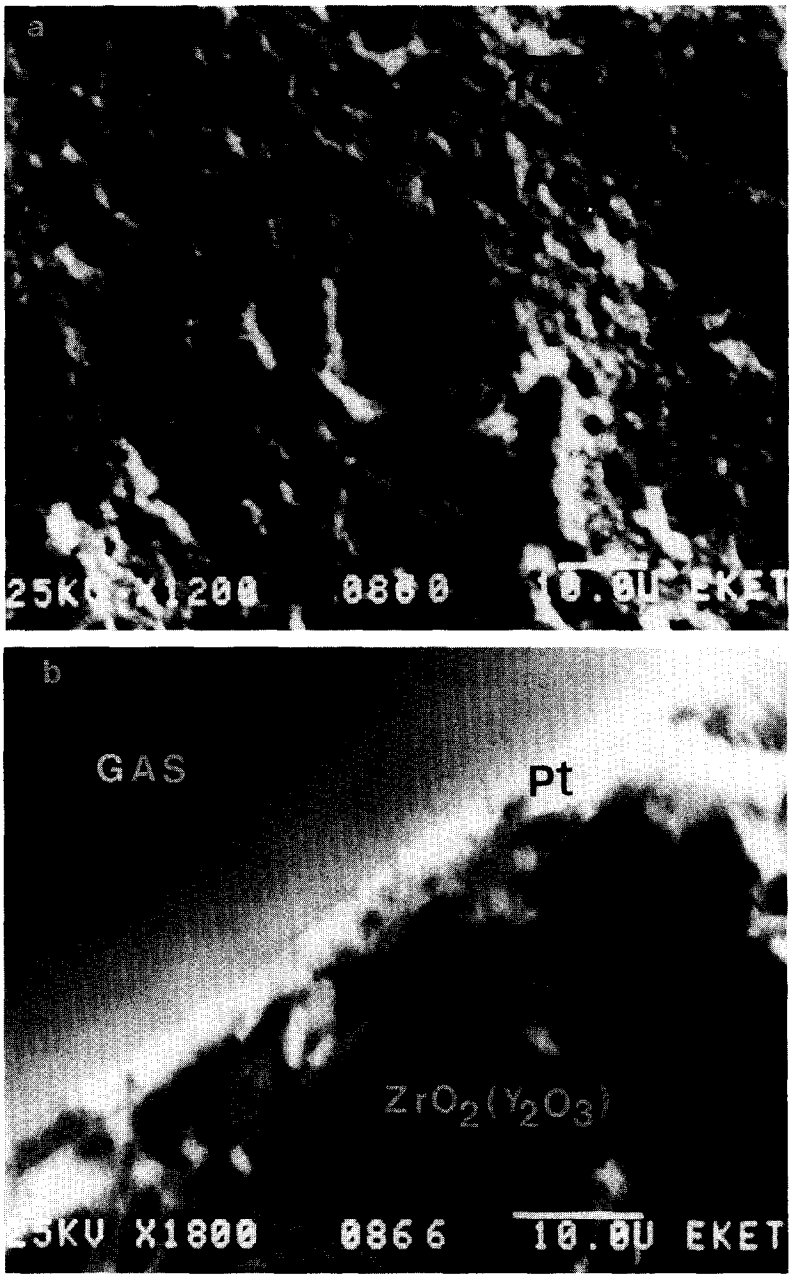

FIG. 3. Scanning electron micrographs of the top side of a porous Pt catalyst film (a) and of a section perpendicular to the Pt catalyst–stabilized zirconia interface (b).

calcining in air first for 2 h at 400°C and then at 820°C for 20 min. Porous Pt catalyst films deposited in this mode have thicknesses on the order of 5 μm and have been shown by XPS to contain no detectable metal impurities (*14, 30*). Figure 3 shows typical scanning electron micrographs of the top side of a porous Pt catalyst film (Fig. 3a) and of a section perpendicular to the Pt catalyst film-stabilized zirconia interface (Fig. 3b). Three catalyst films were used in the course of the experiments. As shown in Table 1 the

TABLE 1

Reactor catalyst	Reactive oxygen uptake of catalyst–electrode (N/g-at. O)	Exchange current density at 400°C, $P_{O_2} = 5.10^{-2}$ bar and $P_{ET} = 4.10^{-3}$ bar $i_0/(\mu A/cm^2)$	Relaxation times	
			Experimental (τ/min)	Computed ((2FN/I)/min)
R1	8.8×10^{-8}	1.3	—	
R2	4.2×10^{-9}	1.3×10^{-6}	6.0(I = 1 μA)	13.5
R3	4.8×10^{-8}	0.37	2.0(I = 100 μA)	1.6

three catalysts differed in their active surface area, which was measured by a surface titration technique described recently (*14*), and in the exchange current density of the catalyst–solid electrolyte interface i_0. The values of i_0 were measured electrochemically as described below.

It was found that particular attention must be paid during catalyst preparation in order to ensure that the catalyst adheres well to the stabilized zirconia and that good electrical contact is established between all the parts of the porous Pt film. When the latter requirement is not met the observed time constants for the cell voltage during galvanostatic transients are very short, typically less than 1 s, and there is no significant rate increase.

Measurement of the Catalyst–Solid Electrolyte Interface Activation Overpotential η and of the Exchange Current Density i_0: Theory and Experimental Procedure

Two porous Pt films were deposited on the outside bottom wall of the stabilized zirconia tube which was exposed to ambient air as shown in Fig. 4. One of the films with a superficial surface area of 1.2 cm^2 served as the counter electrode and the other with a superficial surface area of 0.1 cm^2 served as a reference electrode.

Under open-circuit conditions the film exposed to the reactants (working electrode) functions as a regular catalyst for C_2H_4 oxidation. By measuring its potential relative to the reference or counter electrode, i.e., by using SEP, one can determine the thermodynamic activity of oxygen on the catalyst during reaction (*8–14*), which may differ substantially from the gas-phase oxygen activity if oxygen adsorption is not in equilibrium. When the circuit is closed and a galvanostat (in this work an AMEL 553 galvanostat–potentiostat) is used to apply a constant current I between the working and the counter electrodes, then oxygen anions O^{2-} are transferred to or from the working catalyst–electrode at a rate $I/2F$ where F is Faraday's constant. At the same time the catalyst potential relative to the reference electrode V'_{WR} deviates from its open-circuit emf value $V^0_{WR} = V_{WR}$ ($i = 0$). The difference $V'_{WR} - V^0_{WR}$ equals ideally the overpotential η at the catalyst–solid electrolyte interface (*30, 41*). In practice the reference electrode is never ideal and V'_{WR} always contains a nonzero ohmic component. This component, which was typically on the order of *10–50* mV in our system, was determined using the current interruption technique in conjunction with a Hameg HM 205 memory oscilloscope and

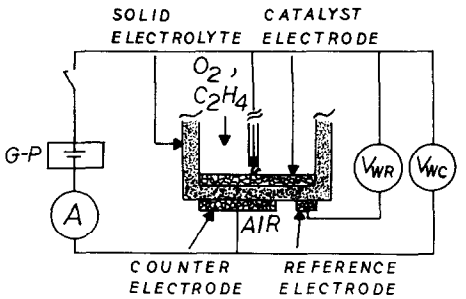

FIG. 4. Catalyst and auxiliary electrodes configuration; G-P, galvanostat–potentiostat.

was subtracted from V'_{WR} in order to obtain the IR-free catalyst potential V_{WR}. This permitted accurate measurement of η from

$$\eta = V_{WR} - V^{\circ}_{WR}. \quad (4)$$

From the experimentally determined dependence of η on the current I through the catalyst–solid electrolyte interface, or equivalently from the dependence of η on the current density $i = I/A$, where A is the solid electrolyte surface area (= 1.5–2.0 cm^2 in our system), one can calculate the exchange current density i_0. This parameter is a measure of the electrocatalytic activity of the catalyst–solid electrolyte interface for the reaction

$$O^{2-} \leftrightharpoons O(a) + 2e^- \quad (5)$$

where O(a) is oxygen chemisorbed on the metal catalyst in the vicinity of the three phase boundaries between the catalyst, the solid electrolyte, and the gas phase. The exchange current density i_0 expresses the rates of the forward and backward reactions (5), which are equal when $I = 0$. The value of i_0 is well known to depend on the coverage θ_0 of chemisorbed oxygen on the catalyst surface (*41, 45*). Moreover, it not only depends on the intrinsic kinetic constants of reaction (5) but is also proportional to the "interline length" of the electrolyte–catalyst–gas phase three-phase boundary. Consequently i_0 depends crucially on the catalyst film porosity and on catalyst crystallite size and morphology. High i_0 values, e.g., 10^{-3} A/cm^2, indicate a nonpolarizable metal–solid electrolyte interface, whereas low i_0 values, e.g., 10^{-12} A/cm^2, imply a highly polarizable interface across which very small current densities i suffice to create high overpotentials η. These are consequences of the classical Butler–Volmer equation

$$i/i_0 = \exp(\alpha_a F\eta/RT) - \exp(-\alpha_c F\eta/RT) \quad (6)$$

which relates i, i_0, and η. The usual way to extract i_0 from η vs i data is through the high field approximation ($\eta > 100$ mV) in which case Eq. (6) reduces to

$$\ln(i/i_0) = \alpha_a(F\eta/RT) \quad (6a)$$

for anodic ($i > 0$, $\eta > 0$) currents and

$$\ln(-i/i_0) = \alpha_c F\eta/RT \quad (6b)$$

for cathodic ones. Thus by plotting ln i vs η (Tafel plot) one obtains i_0 and the anodic and cathodic transfer coefficients α_a and α_c. Such Tafel plots are shown in Fig. 5 for two of the catalysts used in the present investigation. One can then check the accuracy of the extracted i_0, α_a, and α_c values using the low field approximation ($\eta < 10$ mV) in which case Eq. (6) reduces to

$$i/i_0 = (\alpha_a + \alpha_c)F\eta/RT. \quad (6c)$$

The parameters i_0, α_a, and α_c refer to the *electrocatalytic* reaction (5), which takes place at the catalyst–gas–solid electrolyte three-phase boundaries (*39, 41, 45*) and the rate of which, as already mentioned, is several orders of magnitude smaller than the induced changes in the rate of the *catalytic*

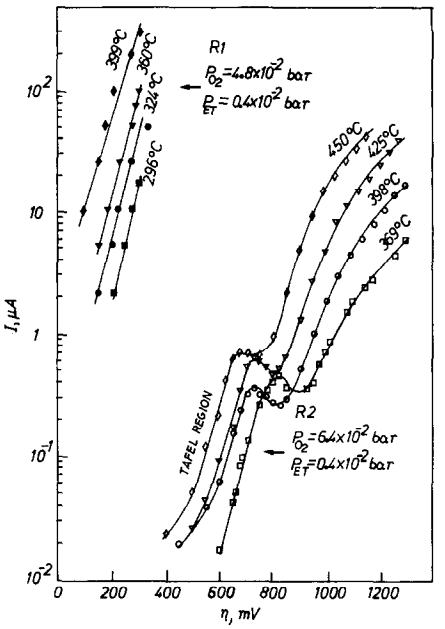

FIG. 5. Tafel plots for the catalyst–solid electrolyte interface.

reaction under study, i.e., C_2H_4 oxidation which occurs over the entire Pt catalyst surface. However, these parameters play an important role in understanding the electrocatalytically induced change in catalytic activity. The parameter which connects the *electrocatalytic* reaction rate, which equals the rate of O^{2-} transport through the electrolyte to or from the catalyst, with the induced dramatic changes in *catalytic* activity for C_2H_4 oxidation, is the overpotential η, which as shown under Discussion section is proportional to the induced change in the work function of the catalyst.

RESULTS

Open-Circuit Kinetic Measurements

In order to obtain a thorough understanding of the effect of O^{2-} pumping on the kinetics of C_2H_4 oxidation on Pt, it is important to describe first the open-circuit ($I = 0$) kinetic behavior. The kinetics of this reaction have been studied by several workers (*12, 31–35*) and one of these studies was performed in the same reactor system with similar porous Pt electrodes but under open-circuit, i.e., regular, catalytic conditions (*12*). In that study it was found that the rate of the reaction r_o (g-at. O/s) could be approximated well by

$$r_o = KK_{ad}P_{ET}P_{O_2}/(KP_{ET} + K_{ad}P_{O_2}), \quad (7)$$

where the subscript o refers to regular (open-circuit) catalytic activity. This kinetic expression, together with the SEP measurements (*12*), had been interpreted quantitatively by the kinetic scheme

$$\tfrac{1}{2}\left\{\begin{array}{l} O_2(g) + S \xrightarrow{K_{ad}} S \cdot O_2 \\ S \cdot O_2 + S \rightarrow 2S \cdot O \end{array}\right\} \quad (8a)$$

$$C_2H_4(g) + O(a) \xrightarrow{K} P \xrightarrow{5/2O_2} 2CO_2 + 2H_2O, \quad (8b)$$

where S denotes a surface site and P is a reactive intermediate which is rapidly oxidized by gaseous or adsorbed oxygen. The nature of such an intermediate has been investigated in a number of recent surface spectroscopic studies (*31, 32, 34*). On the fuel-lean side ($K_{ad}P_{O_2} \gg KP_{ET}$) oxygen adsorption is near equilibrium and step (8b) is rate limiting. Thus Eq. (7) reduces to

$$r_o = KP_{ET}. \quad (9)$$

On the fuel-rich side ($K_{ad}P_{O_2} \ll KP_{ET}$) the surface coverage of oxygen θ_o is low and the rate is controlled by oxygen adsorption. In this case Eq. (7) reduces to

$$r_o = K_{ad}P_{O_2}. \quad (10)$$

In the present work reasonably close agreement was observed between the open-circuit kinetic data and the rate expressions (7), (9), and (10). The observed temperature dependence of the kinetic constants K_{ad} and K is shown in Table 2. The activation energy for oxygen adsorption is 2–6 kcal/mol, i.e., considerably lower than the value reported in Ref. (*12*) but in reasonable agree-

TABLE 2

Temperature Dependence of Open-Circuit Kinetic Parameters

Reactor catalyst	K/s^{-1}	K_{ads}/s^{-1}	T range (°C)	Measured turnover frequency (s^{-1}) at 360°C, $P_{O_2} = 5 \times 10^{-2}$ bar and $P_{ET} = 4 \times 10^{-3}$ bar
R1	$2.1 \times 10^6 \exp(-5500/T)$	$1.4 \times 10^3 \exp(-1000/T)$	300–400	1.7
R2	$6.9 \times 10^{11} \exp(-13000/T)$	$1.7 \times 10^4 \exp(-1500/T)$	370–450	3.47 (369°C)
R3	$7.1 \times 10^6 \exp(-6300/T)$	$3.2 \times 10^5 \exp(-3100/T)$	300–400	1.4
Ref. (*12*)			250–400	1.5

ment with recent work on the oxidation of CO under similar conditions (*14*). The activation energy for C_2H_4 reaction with chemisorbed O is 11–26 kcal/mol which is substantially higher than the value reported in Ref. (*12*). Despite these differences in activation energies, the observed turnover rates are comparable for all three catalysts with those measured in Ref. (*12*) as also shown in Table 2.

Exchange Current Densities

As shown in Fig. 5 and in Table 1, the Pt–solid electrolyte exchange current density i_0 was substantially different in the three catalysts used. This is due to differences in crystallite size and morphology. The temperature dependences of i_0 are, however, similar for all three catalysts and suggest an apparent activation energy of 38–45 kcal/mol, in good agreement with previous studies (*41, 45, 46*). Also, the anodic transfer coefficient α_a was found to equal 1 ± 0.05 for all three catalysts. It should be noted that the i_0 values are obtained from the linear (Tafel) parts of the ln I vs η curves shown in Fig. 5. A linear Tafel plot implies that the surface coverage of electrokinetically important adsorbed species, i.e., atomic oxygen in this system, remains practically constant, since i_0 is strongly dependent on θ_o (*41, 45, 46*). In the case of the linear parts of the curves in Fig. 5 this corresponds to $\theta_o \approx 1$. At higher overpotential in the presence of C_2H_4 there are strong deviations from linearity which also indicate an apparent steady-state multiplicity. This is due to the fact that at this point the steady-state θ_o starts to decrease rapidly due to the very fast reaction of chemisorbed oxygen with ethylene. Details on the exact dependence of i_0 on P_{ET} and P_{O_2} will appear elsewhere (*39*). The major conclusion of this detailed investigation is that ethylene does not react with O^{2-} at the three phase boundaries to any measurable extent so that reaction (5) is the only electrocatalytic reaction which takes place at the catalyst–solid electrolyte-gas phase interline.

The NEMCA Effect: Transients

Figure 6 shows a typical galvanostatic transient, i.e., a typical catalytic rate transient when a constant current I, and thus a constant flux of O^{2-} equal to $I/2F$, is supplied to the catalyst. At the start of the experiment the circuit is open and the catalyst is at a steady-state activity. The reaction rate is $r_o = 1.50 \times 10^{-8}$ g-at. O/s. At time $t = 0$ the galvanostat is used to apply a current $I = 1$ μA with a corresponding rate of oxygen transfer to the catalyst $G_o = I/2F = 5.18 \times 10^{-12}$ g-at. O/s. This causes a roughly 26-fold increase in the rate. The rate increase $\Delta r = 38.5 \times 10^{-8}$ g-at. O/s is a factor of 74,000 greater than G_o. According to the definition of the enhancement factor Λ (Eq. 3),

$$\Lambda = \Delta r / G_o. \tag{11}$$

Thus in this case $\Lambda = 74{,}000$. At the same time the voltage V_{WR} between the catalyst and the reference electrode changes from -150 mV to a steady-state value of 472 mV. Subsequently the circuit is opened and r is restored to its initial value within 90 min. The galvanostat polarity is then reversed and a current -1 μA is applied to the cell with a corresponding rate of oxygen removal from the catalyst $G_o = -5.18 \times 10^{-12}$ g-at. O/s. This has a negligible effect in catalytic reaction rate, although the V_{WR} transient is similar.

Steady-State Effect of Current

Figures 7a and 7b show the steady-state effect of applied current I on the rate of ethylene oxidation with catalysts 1 and 2. In order to facilitate comparison with the rate of O^{2-} transport through the electrolyte ($I/2F$), the rate of ethylene oxidation is always expressed in terms of the rate of atomic oxygen consumption. Figures 7a and 7b show that the enhancement factor Λ is typically on the order of 10^4 for catalyst 1 and 10^5 for catalyst 2. A quantitative expla-

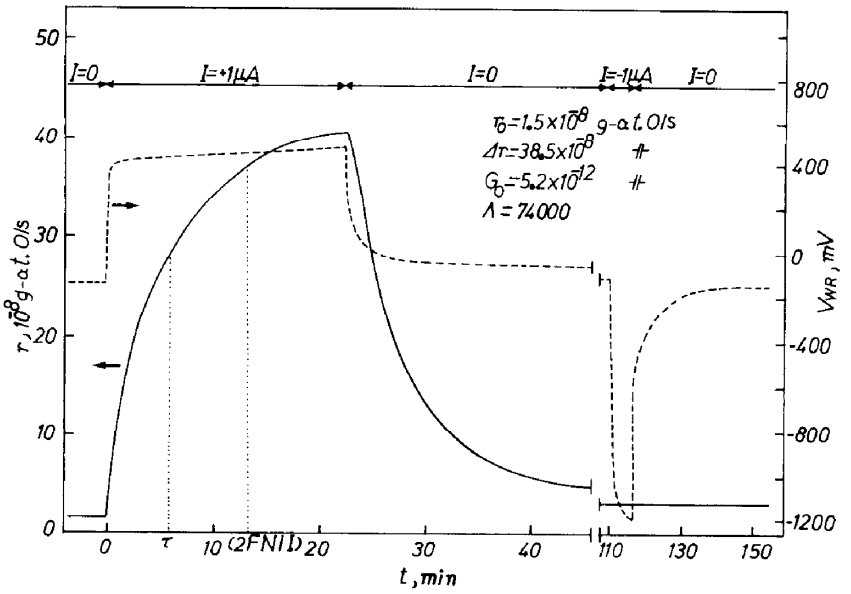

FIG. 6. Rate and catalyst potential response to step changes in applied current; comparison of experimental (τ) and computed ($2FN/I$) relaxation time constants; $T = 370°C$, $P_{O_2} = 4.6 \times 10^{-2}$ bar, $P_{ET} = 3.6 \times 10^{-3}$ bar, catalyst R2. See text for discussion.

nation for the magnitude of Λ and for the differences between catalysts 1 and 2 is given under Discussion.

It should be emphasized that both Figs. 7a and 7b have been obtained with *fuel-lean* gaseous compositions. Consequently the open-circuit catalytic rate r_o is given from Eq. (9); i.e., it is first order in ethylene and

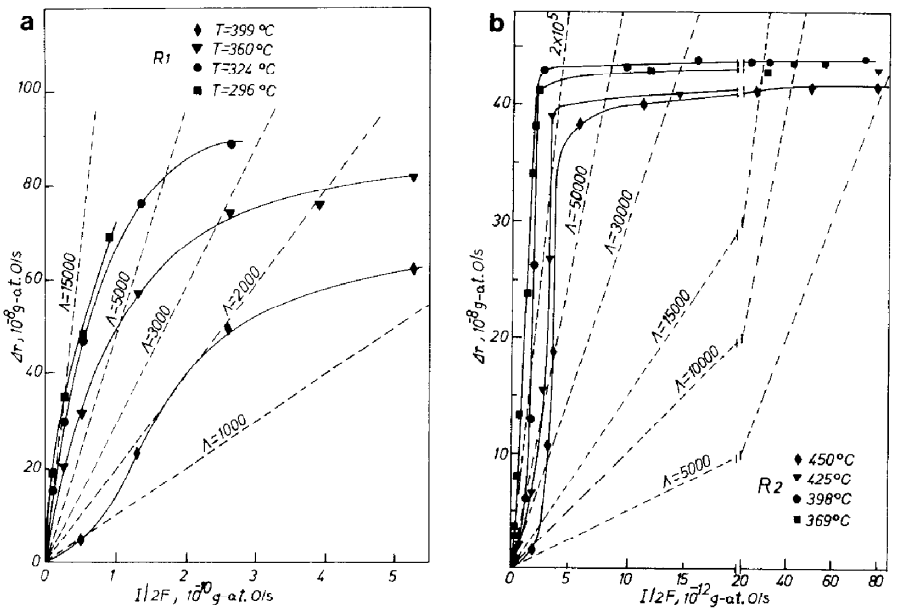

FIG. 7. Steady-state effect of applied current on the rate of C_2H_4 oxidation. Broken lines are constant enhancement factor lines. (a) Catalyst R1, $P_{ET} = 0.4 \times 10^{-2}$ bar, $P_{O_2} = 4.8 \times 10^{-2}$ bar; (b) catalyst R2, $P_{ET} = 0.4 \times 10^{-2}$ bar, $P_{O_2} = 6.4 \times 10^{-2}$ bar.

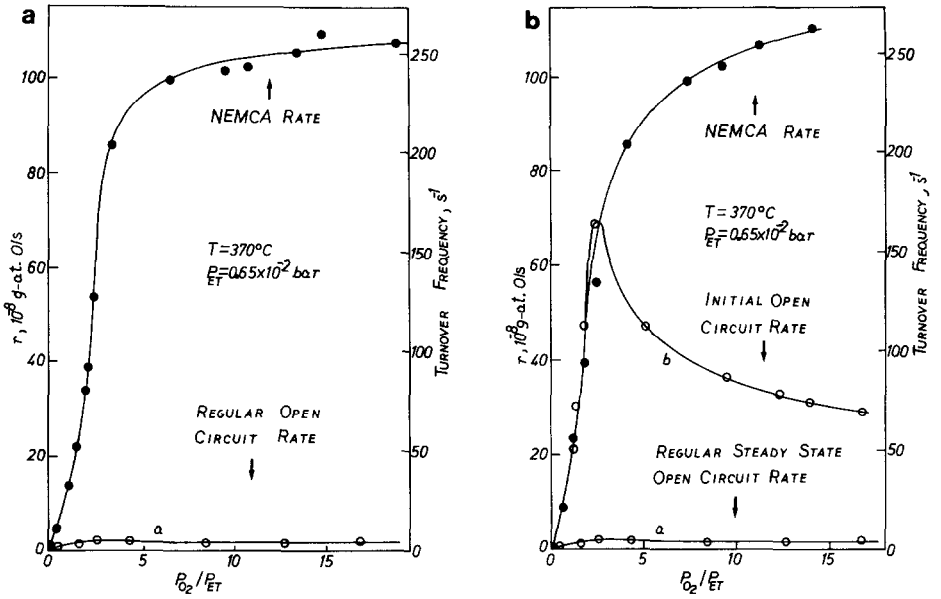

FIG. 8. Effect of gaseous composition on regular (open-circuit) and NEMCA-induced reaction rate (V_{WR} = 1 V). Catalyst R2. (a) Preoxidized surface; (b) prereduced surface.

zeroth order in oxygen, and thus reaction (8b) is rate limiting. It was found that as the rate increases with increasing current, the order of the reaction with respect to C_2H_4 and O_2 does not change until the rate reaches the plateaus shown in Figs. 7a and 7b. When this happens the order of the reaction changes abruptly. The reaction becomes zero order in C_2H_4 and first order in O_2, i.e., $r = K_{ad}P_{O_2}$, and thus the O_2 adsorption step (8a) becomes rate limiting. By further increasing the current there is no rate increase.

Effect of Gaseous Composition and Catalyst Pretreatment

While O^{2-} pumping has such a dramatic effect on the rate on the fuel-lean side, i.e., when $r = KP_{ET}$, it has practically no effect on the rate on the fuel-rich side, i.e., when $r = K_{ad}P_{O_2}$. This is shown in Figs. 8a and 8b which depict the effect of the P_{O_2}/P_{ET} ratio on reaction rate under open-circuit (i = 0, $V_{WR} = V^{o}_{WR}$, η = 0) conditions and at a constant catalyst potential V_{WR} = 1V. Figure 8a was obtained with a preoxidized catalyst surface and shows that while on the fuel-lean side O^{2-} pumping causes a 50-fold increase in reaction rate, i.e., $r/r_o \approx 50$, on the fuel-rich side the effect of O^{2-} pumping practically vanishes. This is depicted even more clearly in Fig. 8b which corresponds to a thoroughly prereduced catalyst surface. On the fuel-rich side O^{2-} pumping has no measurable effect on the rate, while it is $r/r_o \approx 3.5$ on the fuel-lean side. It should be emphasized that the curve labeled (b) in Fig. 8b was obtained within a time frame of approximately 6 h and represents quasi-steady-state measurements as the open-circuit rate eventually stabilizes (within 40–60 h) to the curve labeled (a), which practically coincides with that obtained on a preoxidized surface (Fig. 8a). This is due to the slow formation of surface PtO_2 under oxidizing conditions as discussed in a previous paper (*14*). With the exception of the quasi-steady-state measurements of curve (b) in Fig. 8b, all other kinetic results reported here are stable steady-state results.

This dramatically different behavior between the fuel-lean and the fuel-rich sides shows that O^{2-} pumping has practically no effect on the oxygen adsorption kinetic

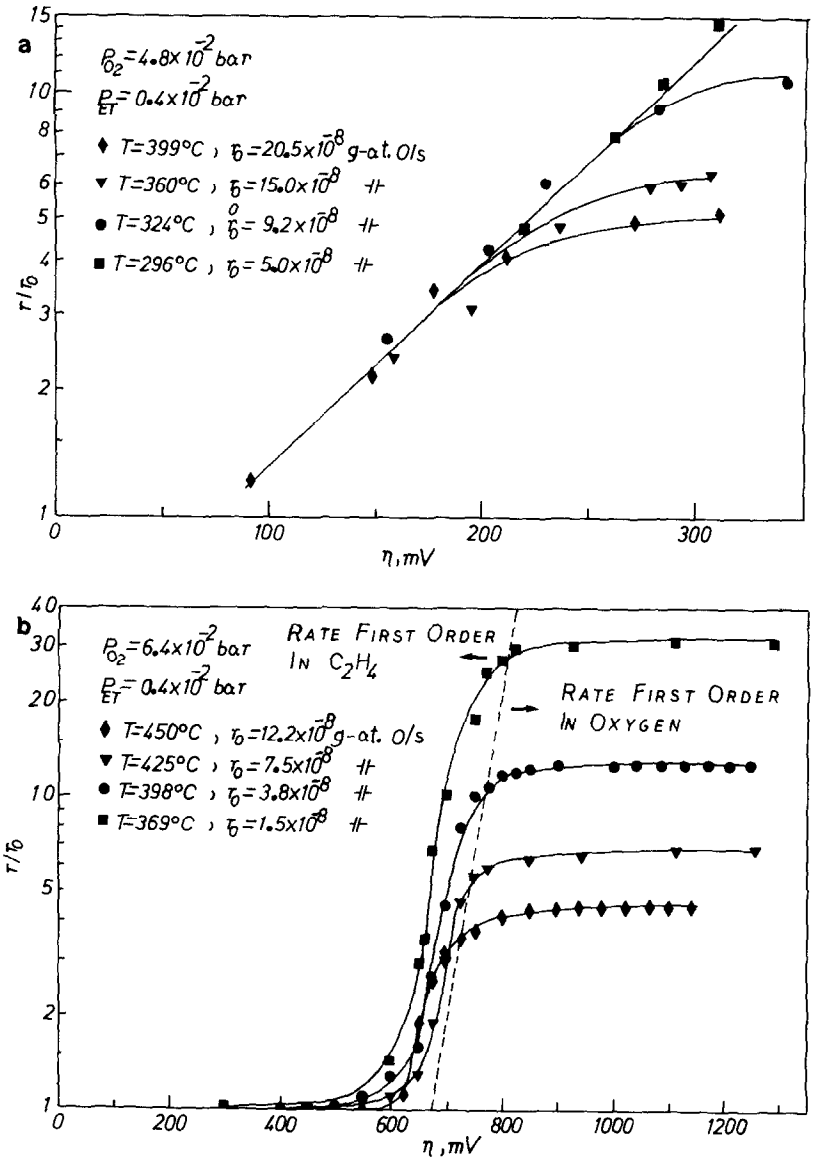

FIG. 9. Effect of catalyst–solid electrolyte activation overpotential η on the rate of C_2H_4 oxidation. (a) Catalyst R1; (b) catalyst R2.

constant K_{ad} and has a very pronounced effect on the kinetic constant K for the reaction between ethylene and chemisorbed oxygen. This is shown more clearly below and is explained under Discussion.

Effect of Overpotential

Figures 9a and 9b show the same data presented in Figs. 7a and 7b, but in terms of $\ln(r/r_o)$ vs η. Below a certain threshold η value, which we denote by η^*, the rate is practically unaffected, but when η exceeds η^* the rate increases exponentially with η, i.e.,

$$\ln(r/r_o) = C(\eta - \eta^*); \quad \eta > \eta^*. \quad (12)$$

This exponential increase continues until the point where the rate becomes zeroth

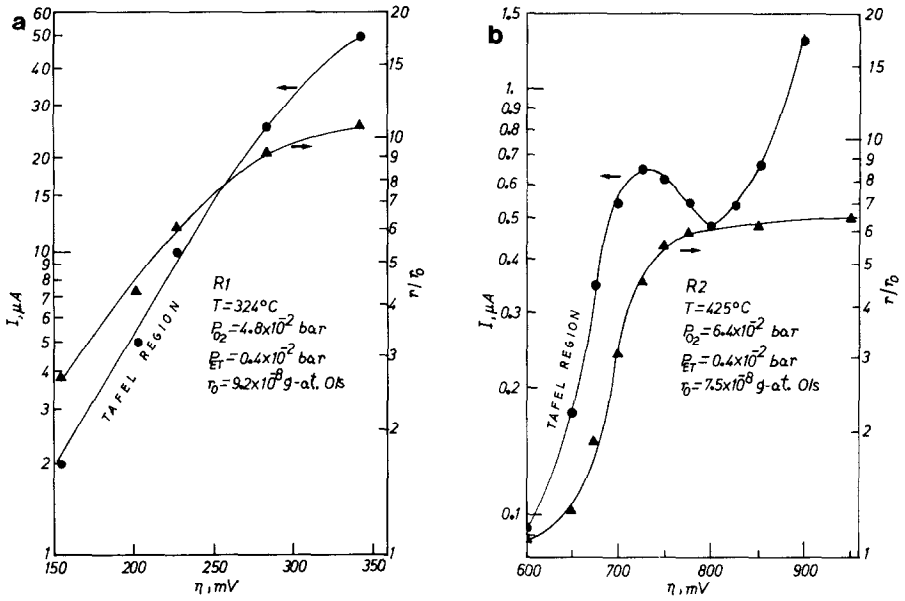

FIG. 10. Effect of overpotential on current and on the rate of C_2H_4 oxidation. (a) Catalyst R1; (b) catalyst R2.

order in C_2H_4 and first order in O_2 is reached, i.e., $r = K_{ad}P_{O_2}$. At this point the rate is typically 10 to 30 times higher than the open-circuit rate r_o. The measured η^* values were substantially different for the two catalysts R1 and R2. However, the constant C was on the order of F/RT for both catalysts as discussed below.

The exponential increase in reaction rate with η coincides with the linear part of the Tafel plots. This is shown in Fig. 10 and emphasizes that the exponential rate increase with η takes place at practically constant surface oxygen coverage θ_o. This shows again that it is the kinetic constant K which increases exponentially with η.

Effects of Catalyst Potential V_{WR}

The observed threshold η^* values were substantially different for catalysts R1 and R2. However, the measured open-circuit emf values V^o_{WR} were also different for the two catalysts over a wide range of conditions. The reason for these differences is not obvious and must be related to the different i_0 values of the two catalysts (Table 1). However, the differences between η^* and V^o_{WR} tend to cancel out, so that when the two catalysts are examined at similar potentials V_{WR} their behavior is similar. This is shown in Fig. 11 where ln K is plotted vs the dimensionless parameter Π, defined as

$$\Pi = FV_{WR}/RT. \tag{13}$$

Despite some scattering, this mode of presentation tends to bring together all the results not only for different temperatures and gaseous compositions with the same catalyst but also for the two different catalysts which exhibit substantially different values of i_0, V^o_{WR}, and surface area. Thus all the data can be approximated by

$$\ln(K/K_o) = \alpha F(V_{WR} - V^*_{WR})/RT; \quad V_{WR} > V_{WR}, \tag{14}$$

where $\alpha = 0.5 \pm 0.05$ and 1.0 ± 0.1 for catalysts R1 and R2. The corresponding V^*_{WR} values are -110 and 102 mV, respectively. Defining a dimensionless parameter Π' as

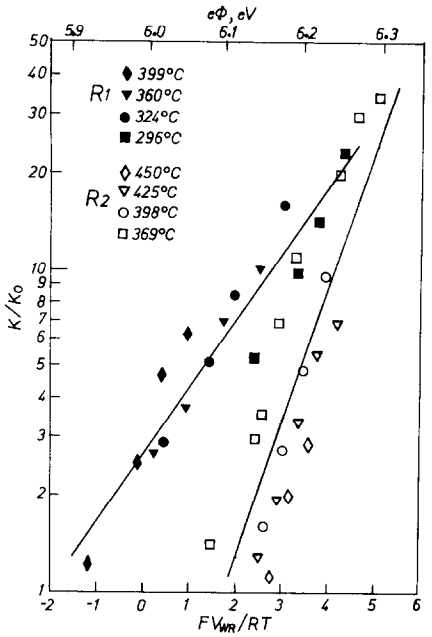

FIG. 11. Effect of catalyst potential V_{WR} and corresponding work function value on the kinetic constant K of C_2H_4 oxidation on Pt. See text for discussion. The open-circuit (K_o) values can be computed from Fig. 9 and Eq. (9).

$$\Pi' = F(V_{WR} - V^*_{WR})/RT \qquad (15)$$

one can rewrite Eq. (14) as

$$\ln(K/K_o) = \alpha\Pi'; \ \Pi' > 0 \quad \text{and} \quad K = K_o; \ \Pi' \leq 0. \qquad (16)$$

As shown under Discussion, V_{WR}, and consequently Π, is proportional to the deviation $e\Delta\Phi$ of the catalyst work function from its value at the reference electrode which is in contact with O_2. The second abscissa axis in Fig. 11 gives an approximate estimate of the catalyst work function $e\Phi$. It is constructed on the assumption that chemisorbed oxygen on the reference electrode causes a negative surface potential of 1 V, i.e., an increase of 1 eV in the average work function of Pt with respect to vacuum conditions (*42*).

Global Kinetic Behavior

Although O^{2-} pumping has such a dramatic effect on the kinetic constant K, it has no detectable effect on the oxygen adsorption constant K_{ad} or on the reaction mechanism. This is shown conclusively in Figs. 12a and 12b which demonstrate that the rate equation (7), which was obtained from open-circuit measurements, can also provide a quantitative fit to the NEMCA-induced kinetic behavior of both catalysts. Substituting K from Eq. (16) into Eq. (7) and assuming K_{ad} to be unaffected, one obtains

$$r = K_{ad}K_oP_{ET}P_{O_2}\exp(\alpha\Pi')/[K_oP_{ET}\exp(\alpha\Pi') + K_{ad}P_{O_2}] \qquad (17)$$

which can be rewritten in the linearized form

$$P_{O_2}/r = K_{ad}^{-1} + (P_{O_2}/P_{ET})K_o^{-1}\exp(-\alpha\Pi'). \qquad (18)$$

As shown in Figs. 12a and 12b Eq. (18) is in very good agreement with experiment for both catalysts. It can be therefore concluded that the kinetic scheme of reactions (8a) and (8b) can adequately describe both the regular (open-circuit) and the NEMCA-induced catalytic activity of Pt for the oxidation of C_2H_4.

NEMCA Effect on Activation Energies and Preexponential Factors

By studying the temperature dependence of r at various constant overpotentials η on the fuel-lean side, i.e., when $r = KP_{ET}$, and by using standard Arrhenius ln K vs $(1/T)$ plots, one can examine the effect of η on the activation energy E and on the preexponential factor K° of the Eley–Rideal kinetic constant K ($= K^\circ\exp(-E/k_bT)$) of the reaction (8b) between gaseous ethylene and chemisorbed oxygen. It was found that O^{2-} pumping to the catalyst causes a significant (up to 60%) decrease in E and a concomitant decrease in K°. This is shown in Figs. 13a and 13b where E and $k_bT\ln K^\circ$ are plotted vs $e\eta$. As shown in these figures there is a linear decrease in E and in ln K° when η exceeds the threshold value of η^*. The slopes α_H of the E vs $e\eta$ plots are -1.1 and

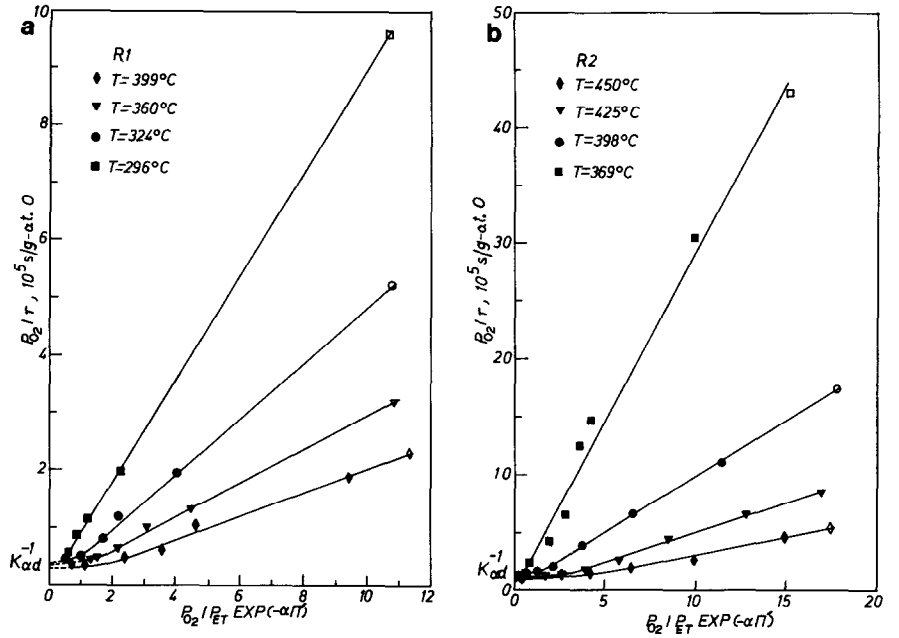

FIG. 12. Effect of gaseous composition and $\Pi' = F(V_{WR} - V^*_{WR})/RT$ on the kinetic behavior of C_2H_4 oxidation. Open symbols, regular (open-circuit) rate; solid symbols, NEMCA rate. (a) Catalyst R1; (b) catalyst R2.

-4.3 respectively for R1 and R2. It can therefore be concluded that the dramatic increase in K is due to a lowering of the activation energy, which by far counterbalances the compensating decrease in the preexponential factor. The corresponding

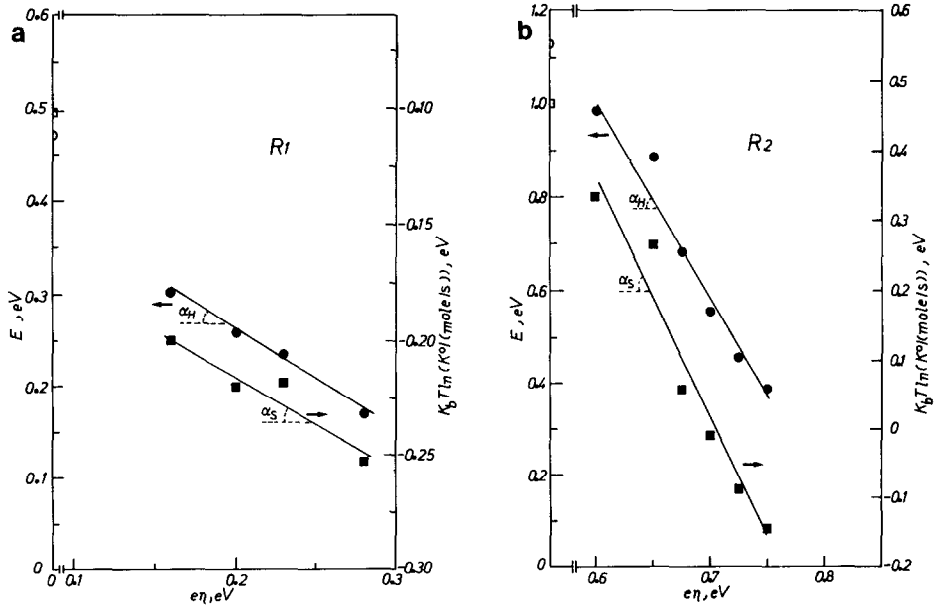

FIG. 13. Effect of overpotential on the activation energy and preexponential factor of the kinetic constant K. (a) Catalyst R1; (b) catalyst R2.

slopes α_s of the $k_bT \ln K^o$ vs $e\eta$ plots are -0.4 and -3.5 respectively for R1 and R2. The measured α_H and α_s values differ between the two catalysts, but were found to satisfy $\alpha = \alpha_s - \alpha_H$ within 20%. This shows the consistency of the extracted activation energy and preexponential factor values.

DISCUSSION

Main Results

1. The rate of C_2H_4 oxidation on Pt can be enhanced up to a factor of 50 by supplying O^{2-} to the catalyst surface. The observed increase in catalytic reaction rate is 10^4 to 10^5 higher than the rate of O^{2-} transport to the catalyst.

2. Oxygen anion O^{2-} pumping affects only the kinetic constant K of the Eley–Rideal step between gaseous ethylene and chemisorbed oxygen and *not* the kinetic constant K_{ad} of oxygen adsorption. Consequently the overall rate is affected only when $KP_{ET}/K_{ad}P_{O_2} \ll 1$, i.e., when the rate-controlling step is the reaction of gaseous ethylene with adsorbed oxygen.

3. The kinetic constant K increases exponentially with the catalyst potential according to

$$\ln(K/K_o) = \alpha e(V_{WR} - V^*_{WR})/k_bT = \alpha F(V_{WR} - V^*_{WR})/RT \equiv \alpha\Pi'. \quad (14)$$

Consequently the total kinetic behavior is described quantitatively by

$$r = K_{ad}K_oP_{ET}P_{O_2} \exp(\alpha\Pi')/[K_oP_{ET} \exp(\alpha\Pi') + K_{ad}P_{O_2}]. \quad (17)$$

The oxygen adsorption kinetic constant is not affected by O^{2-} pumping.

Mechanistic Considerations

The kinetic expression (17), which provides a quantitative description of the effect of P_{ET}, P_{O_2}, T, and catalyst potential V_{WR} on catalyst activity, can be interpreted by the same mechanism (12) which describes the open-circuit kinetics, i.e., the one given by Eqs. (8) and by taking into account that the rate constant K of reaction (8b) is given by Eq. (14). Note that Eq. (17) correctly predicts that V_{WR}, or Π', has no effect on the rate on the fuel-rich side, i.e., when $KP_{ET}/K_{ad}P_{O_2} \gg 1$. This is reasonable in view of the fact that changes in the electronic properties of the Pt catalyst will have only a negligible effect on the sticking coefficient of oxygen and on the rate of oxygen adsorption, which is essentially nonactivated, as shown by the temperature dependence of K_{ad} (Table 2).

The successful fit of all the kinetic data with Eq. (17) shows conclusively that O^{2-} pumping to the catalyst does not alter the catalytic reaction mechanism, but simply induces a dramatic increase in the rate constant K of reaction (8b).

Prediction of the Enhancement Factor Λ

The magnitude of the enhancement factor Λ can be obtained as follows: We start by noting that on the fuel-lean side

$$\ln(r/r_o) = \alpha[F(V_{WR} - V^*_{WR})/RT] = \alpha[F(\eta - \eta^*)/RT]. \quad (19)$$

To the extent that $\Delta r \gg r_o$ one can write

$$\ln(\Delta r/r_o) = \alpha[F(\eta - \eta^*)/RT]. \quad (20)$$

From the high-field approximation of the Butler–Volmer equation

$$\ln(i/i_0) = \alpha_a(F\eta/RT). \quad (6a)$$

Subtracting Eqs. (20) and (6a) and using the definition of Λ, i.e., $\Lambda = \Delta r/(I/2F)$, one obtains

$$\Lambda = (2Fr_o/I_o) \exp[(\alpha - \alpha_a)F(\eta - \eta^*)/RT] \exp[-\alpha_aF/RT)\eta^*] \quad (21)$$

with $I_o = i_0A$, where A is the electrolyte surface area. The parameter $I^o = I_o \exp(\alpha_aF\eta^*/RT)$ expresses the current at an overpotential equal to η^*. Consequently Eq. (21) can be rewritten alternatively as

$$\Lambda = (2Fr_o/I^o) \exp[(\alpha - \alpha_a)F(\eta - \eta^*)/RT)]. \quad (22a)$$

If the NEMCA coefficient α does not differ substantially from the anodic transfer

TABLE 3

Comparison of Predicted and Measured Enhancement Factor Λ Values at $T = 400°C$ and $\eta - \eta^* = 150$ mV

Reactor catalyst	$i_0/(\mu A/cm^2)$	$i^0/(\mu A/cm^2)$	Λ (Eq. (22a))	Λ (Eq. (22b))	Λ_{exp}
R1	1.3	2.6	2.4×10^3	7.6×10^3	1.2×10^3
R2	1.3×10^{-6}	3.2×10^{-2}	1.15×10^5	1.15×10^5	1.9×10^5

coefficient α_a, then the last equation reduces to

$$\Lambda \approx 2Fr_o/I^o. \quad (22b)$$

Equations (22a) and (22b) are in good agreement with the experimental Λ values as shown by a typical comparison in Table 3. These equations show that in order to obtain a high Λ value, i.e., a strong non-Faradaic enhancement, one needs a fast catalytic reaction (high r_o) and a highly polarized metal–solid electrolyte interface, i.e., low I_o and I^o values.

The usefulness of Eqs. (22a) and (22b) is not restricted to the reaction of ethylene oxidation on Pt. They have also been found to describe well the magnitude of Λ in all the other reactions where the NEMCA effect has been studied. These reactions are listed in Table 4 together with the Λ values measured. Detailed kinetic results will be presented in separate papers (*36–39*).

A common feature of all these studies is that over certain ranges of catalyst potential the rates of catalytic reactions increase exponentially with catalyst potential V_{WR}.

The Origin of the NEMCA Effect and of the Exponential Dependence of Catalytic Rate on V_{WR}

In order to explain the experimental observation

$$\ln(K/K_o) = \alpha F(V_{WR} - V^*_{WR})/RT, \quad (14)$$

which has been found to describe the NEMCA effect both for the present work and for all other systems where the effect of O^{2-} pumping on catalysts has been studied with simultaneous accurate measurement of the overpotential η and of the catalyst potential V_{WR} (*36–39*), one must first examine the effects of O^{2-} pumping and of the appearance of activation overpotential η on the electronic properties of the metal catalyst.

The appearance of activation overpotential η at the catalyst–solid electrolyte interface implies that the overall reaction

TABLE 4

List of Catalytic Reactions Found to Exhibit the NEMCA Effect

Reactants	Products	Catalyst	T (°C)	Λ Values	Reference
$CH_2 = CH_2$, O_2	Ethylene oxide CO_2	Ag	320–420	<300	(*27, 28*)[a]
Propylene, O_2	Propylene oxide CO_2	Ag	320–420	<300	(*29*)[a]
CO, O_2	CO_2	Pt	300–550	<500	(*30*)
CH_3OH	H_2CO, CO, H_2	Ag	550–700	−10	(*36*)[a]
CH_3OH, O_2	CO_2, H_2CO	Pt	400–500	<12,000	(*38*)[a]
$CH_2 = CH_2$, O_2	CO_2, H_2O	Pt	260–420	$<3 \times 10^5$	This work

[a] Change in product selectivity observed.

$$O^{2-} \rightarrow O(a) + 2e^- \quad (23)$$

is slow and rate limiting for the transfer of O^{2-} from the counter electrode to the catalyst. This means that an excess of O^{2-} is accumulating at the three phase boundaries between the solid electrolyte, the gas phase, and the catalyst. It is well known (*42*) that negatively charged ions forced to adsorb on a metal surface, in this case Pt, cause a negative surface potential change $\Delta\chi$ and consequently an increase in the metal work function $e\Delta\Phi$.

One might expect that this change in $e\Delta\Phi$ would be restricted to those metal crystallites which are in actual contact with the zirconia and therefore in direct contact with excess O^{2-}. However, one is faced with the following experimental observation.

The relaxation time constant τ, defined as the time required for the rate increase Δr to reach 63% of its steady-state value during a galvanostatic transient (*28, 30*), is $2FN/I$ where N is the *total* number of surface metal gram-atoms (Fig. 6 and Table 1). This shows that *all* the Pt crystallites change their catalytic activity, even though most of them are not in contact with the ZrO_2 and some are 50,000 Å away from it. Therefore some species resulting from reaction (23) is spreading over the entire catalyst surface; i.e., there is a spillover effect. What could that species be? Certainly not O(a), since the surface coverage of adsorbed oxygen is near unity under fuel-lean conditions where the rate increases exponentially with V_{WR}. It might be O^{2-}, but this can be shown (*39, 41, 46*) to be inconsistent with the measured transfer coefficient $\alpha_a = 1$, unless one postulates that two electrons are removed *simultaneously* from O^{2-} in the rate-limiting step of reaction (23) and that this deelectronation step takes place not at the three phase boundaries but anywhere on the Pt catalyst surface (*39*). This is a very unlikely possibility and cannot explain the well-established increase in the exchange current density i_0 with increasing three-phase boundary length. Furthermore it cannot explain the observed differences between the relaxation time constants of V_{WR} and Δr during galvanostatic transients. The most plausible explanation is that the species diffusing over the entire catalyst surface is O^- resulting from the first elementary step of reaction (23), i.e.,

$$O^{2-} \rightarrow O^- + e^-. \quad (24)$$

If the second elementary step, i.e.,

$$O^- \rightarrow O(a) + e^- \quad (25)$$

is slower than step (24), then O^- is created at the three phase boundaries and can then diffuse over the entire catalyst surface. This is consistent both with the transfer coefficient $\alpha_a = 1$ found by previous workers (*41, 46*) and also measured in this work (both with and without ethylene present in the reactor (*39*)), and with the recent work of Arakawa *et al.* (*43*), who used *in situ* XPS to examine the surface of a Ag film subject to O^{2-} pumping in a ZrO_2 cell and found the appearance of O^- on the Ag surface. The peak would disappear when the current was switched off. It appears therefore that the catalyst work function is changing not only because of the interaction of O^{2-} with the Pt crystallites in immediate contact with the zirconia but also because of the interaction between all the Pt crystallites and O^- ions, which spill over the entire surface within a time constant of $2FN/I$. Some of these oxygen anions O^- which are continuously formed by reaction (24) will eventually lose their charge on the Pt surface by reaction (25) or react with C_2H_4 at a slow rate, so that a steady-state O^- surface concentration is established on the Pt surface.

During a galvanostatic transient this coincides with the eventual stabilization of the catalytic reaction rate to its NEMCA-induced steady-state value.

The next problem is that of quantifying the change in catalyst work function $e\Delta\Phi$ caused by the interaction of the catalyst surface with O^{2-} and O^-. The measured catalyst potential V_{WR} is by definition the

difference between the inner, or Galvani, potential of the catalyst ϕ_W and the reference electrode ϕ_R,

$$V_{WR} = \phi_W - \phi_R. \quad (26)$$

The Galvani potential is the difference between the chemical μ_e and electrochemical potentials $\bar{\mu}_e$ of electrons in a metal; therefore

$$eV_{WR} = (\mu_{e,W} - \mu_{e,R}) - (\bar{\mu}_{e,W} - \bar{\mu}_{e,R}). \quad (27)$$

The chemical potential of electrons μ_e is a pure bulk property and since the catalyst and the reference electrode are made of the same metal and are at the same temperature, it is $\mu_{e,W} = \mu_{e,R}$; therefore

$$eV_{WR} = \bar{\mu}_{e,R} - \bar{\mu}_{e,W}. \quad (28)$$

The electrochemical potential of electrons in a metal is equal by definition to the Fermi level E_F of electrons in the metal (42); therefore Eq. (28) can be rewritten as

$$eV_{WR} = E_{F,R} - E_{F,W}. \quad (29)$$

Thus a positive V_{WR} which corresponds to O^{2-} being pumped to the catalyst surface causes a lowering in the Fermi levels of electrons in the catalyst.

The electrochemical potential $\bar{\mu}_e$ or equivalently the Fermi level E_F is related to the catalyst work function $e\Phi$ by the defining equation of work function, (42), i.e.,

$$e\Phi = -\bar{\mu}_e - e\Psi, \quad (30)$$

where Ψ is the outer, or Volta, potential of the metal. The Ψ potential is nonzero only when there exists a net charge on the metal catalyst. Combining Eqs. (28) and (30) one obtains

$$V_{WR} = (\Phi_W - \Phi_R) + (\Psi_W - \Psi_R). \quad (31)$$

Equation (31) is valid under both open-circuit and closed-circuit conditions. For open-circuit (i.e., SEP) measurements it implies that the open-circuit emf V°_{WR} provides a measure of the catalyst work function in relation to the reference electrode work function provided that no net charge develops on the two electrons, i.e., $\Psi_W = \Psi_R = 0$. Under closed-circuit conditions, i.e., during O^{2-} pumping, the reference electrode remains unaffected; i.e., Φ_R and Ψ_R remain constant. One can therefore rewrite Eq. (31) as

$$\eta = V_{WR(i)} - V_{WR(i=0)} = (\bar{\mu}_{e,W(i=0)} - \bar{\mu}_{e,W(i)})/e = (\Phi_{W(i)} - \Phi_{W(i=0)}) + (\Psi_{W(i)} - \Psi_{W(i=0)}). \quad (32)$$

Equation (32) has been derived rigorously and without making any assumptions. In order to further exploit Eq. (32) it is necessary to examine the magnitude of the Volta potential term $\Psi_{W(i)} - \Psi_{W(i=0)}$ on the catalyst surface exposed to the gas phase. It is important to note that, unlike electrodes used in aqueous electrochemistry where usually the entire electrode surface is in contact with the electrolyte, the catalyst–electrode surface used here is divided in two distinct parts: One part with a surface area on the order of 1 cm^2, which accounts for less than 1% of the total catalyst–electrode surface area, is in actual contact with the electrolyte. The other part, with a surface area on the order of 200 cm^2, is *not* in contact with the electrolyte, but is exposed to the gas phase and constitutes the *catalytically* active surface area. It is worth noting that $\bar{\mu}_{e,W}$ must be the same throughout the bulk of the metal catalyst. However, Φ_W and Ψ_W, a the sum of which equals $-\bar{\mu}_{e,W}/e$, need not be the same over the entire catalyst surface if the catalyst–electrode carries a net charge which is not uniformly distributed on the catalyst surface. Such a charge will, in general, exist but will be localized at the metal–solid electrolyte interface, which is usually modeled as a resistor and a capacitor connected in parallel. However, what is of interest here are changes in Φ_W and Ψ_W on the metal–electrode surface which is catalytically active, i.e., which is exposed to the gas phase. Any ions or molecules directly adsorbing on the catalytically active surface will be paired with a compensating charge

in the metal. The effect of such ion–electron pairs produced by adsorption from the gas phase would be included in a work function measurement and therefore must be included within Φ_W and not Ψ_W. Consequently when the Φ_W and Ψ_W terms in Eqs. (31) and (32) refer to the catalytically active surface of the catalyst electrode, then the Ψ_W terms vanish and one can rewrite these equations as

$$V_{WR} = \Phi_W - \Phi_R \quad (33)$$

$$V_{WR(i)} - V^0_{WR} = \Phi_{W(i)} - \Phi_{W(i=0)}. \quad (34)$$

It must be emphasized again that the Φ terms in Eqs. (33) and (34) refer to the catalytically active surface. The derivation of Eqs. (33) and (34) from Eqs. (31) and (32) appears straightforward. However, the exact validity of Eqs. (33) and (34) must be checked experimentally, e.g., by directly measuring $e\Phi$ by a Kelvin probe. The exact validity of Eqs. (33) and (34) is not a necessary requirement for explaining the NEMCA effect. If only a fraction f of V_{WR} (Eq. (32)) results in a change in Φ and the remaining part $(1 - f)$ results in a change in Ψ, then one obtains Eqs. (33) and (34) with the V_{WR} terms multiplied by f. Nevertheless the striking qualitative and quantitative similarity between oscillations in V_{WR} measured electrochemically (*14, 30*) and oscillations in Φ_W measured by a Kelvin probe (*44*) during CO oxidation rate oscillations on Pt (*14, 30, 44*) provides another strong support that it is $f = 1$ and that Eqs. (33) and (34) are almost exactly valid.

It can be therefore concluded that O^{2-} pumping to or from the catalyst respectively causes an increase or decrease in the catalyst work function $e\Phi$. The magnitude of the increase or decrease is given by Eq. (34). One then has a convenient tool for varying the work function of metal catalysts. The remaining problem is to examine why such a variation in work function should result in an exponential change of catalytic activity of the type described by Eq. (14), which in view of Eq. (34) can be written in the form

$$\ln(K/K_o) = \alpha(e\Phi - e\Phi^*)/k_bT, \quad (35)$$

where $e\Phi^*$ is the catalyst work function at a potential equal to V^*_{WR}.

An answer to this question can be provided starting from the early theoretical work of Boudart (*47*), who explained previous experimental results and showed that the expected change in the heat of adsorption $(-\Delta H_{ad})$ of covalently bonded species when the substrate work function changes by $e\Delta\Phi$ should equal $-(n/2)e\Delta\Phi$, i.e.,

$$\Delta(-\Delta H_{ad}) = -(n/2)e\Delta\Phi, \quad (36)$$

where n is the number of valence electrons of the adatom taking part in the bonding. Equation (36) has been criticized for its simplicity (*42*) but has been found to be in good agreement with experiment (*47*). Consequently for the case of oxygen chemisorption on Pt, $n = 2$ and one would expect

$$(-\Delta H_{ad})_i - (-\Delta H_{ad})_{i=0} = e(\Phi_{W,i-0} - \Phi_{W,i}). \quad (37)$$

It should be noted that according to the Eley–Rideal type kinetic scheme of Eqs. (8) which describes adequately the kinetic behavior of ethylene oxidation both under open-circuit conditions and during O^{2-} pumping (Fig. 12), dissociatively chemisorbed oxygen is the only kinetically important species which is strongly bonded to the catalyst surface. Consequently the NEMCA-induced change in catalyst work function will affect the ethylene oxidation kinetics by a change in the strength of the platinum–oxygen bond. Equation (37) predicts a substantial decrease in the heat of adsorption of oxygen with increasing metal work function. Consequently chemisorbed oxygen becomes progressively more loosely bonded to the catalyst surface as the work function increases; therefore, it is much more susceptible to reaction with gaseous ethylene, as is experimentally observed. Furthermore if one assumes that the nature of the surface activated complex

for the reaction of ethylene with chemisorbed oxygen does not change significantly during O^{2-} pumping, one would expect a lowering in the activation energy of the reaction that would be equal to the increase in catalyst work function, i.e.,

$$\Delta E = \Delta(-\Delta H_{ad}) \approx -\Delta e\Phi_W = -\Delta e V_{WR}. \quad (38)$$

This is definitely an oversimplified picture, yet the experiments (Fig. 13) show that indeed there is a linear decrease in E with V_{WR} for

$$V_{WR} > V^*_{WR}, \quad \text{i.e., } E = E^o + \alpha_H e(V_{WR} - V^*_{WR}), \quad (39)$$

where the parameter α_H takes values of order -1 to -4. It appears therefore that the above simplistic physical model provides at least a qualitative explanation of the NEMCA effect. If the above picture were exactly true it would be $\alpha_H = -1$.

Since chemisorbed oxygen becomes more loosely bonded as V_{WR} increases, one expects an increase in its entropy and a consequent decrease in the preexponential factor K^o. For modeling purposes, but also the basis of Fig. 13, one can assume

$$k_b T \ln(K^o/K^o_o) = \alpha_s e(V_{WR} - V^*_{WR}), \quad (40)$$

where α_s is a parameter similar to the enthalpic parameter α_H but accounting for the entropic changes of chemisorbed oxygen. Substituting Eqs. (39) and (40) into

$$K = K^o \exp(-E/k_b T), \quad (41)$$

one obtains

$$\ln(K/K_o) = (\alpha_s - \alpha_H)e(V_{WR} - V^*_{WR})/k_b T = (\alpha_s - \alpha_H)F(V_{WR} - V^*_{WR})/RT, \quad (42)$$

which is in excellent agreement with the experimental Eq. (14) with

$$\alpha = \alpha_s - \alpha_H. \quad (43)$$

The experimental α, α_s, and α_H values indeed satisfy Eq. (43) within ±20%.

The very good agreement between experiment and the above theoretical considerations does not necessarily prove the validity of the several simplifying assumptions made to derive Eq. (42). However, the fact that these considerations work equally well for all the other reactions, in which the NEMCA effect was studied (Table 4) shows that they can be used as a working hypothesis for the quantitative explanation of the NEMCA effect until new theoretical improvements become necessary.

On the basis of the interesting similarity between Eqs. (14), (35), and (42) which describe the NEMCA effect and Eq. (6a) which is the high-field approximation of the Butler–Volmer equation one might be tempted to seek alternative, purely electrochemical, explanations of the NEMCA effect. However, the facts that (a) the relaxation time constants during galvanostatic transients are on the order of $2FN/I$ where N is the *total* number of surface metal catalyst gram-atoms (Fig. 6 and Table 1) and (b) the observed enhancement factors Λ are proportional to r_o, thus proportional to N and to catalyst surface area and inversely proportional to I^o (Eq. (22b)) and thus to I_o, clearly rule out any such possibility. These observations show conclusively that the NEMCA effect is a catalytic effect taking place over the entire catalyst surface. The effect is induced by a much slower electrocatalytic reaction which occurs at the catalyst–electrolyte–gas phase three-phase boundaries.

CONCLUSIONS

The catalytic activity of Pt for the oxidation of C_2H_4 can be affected dramatically by electrochemically pumping oxygen anions onto the catalyst surface. The induced non-Faradaic electrochemical modification of catalytic activity (NEMCA) leads to rate enhancements up to 5000%. The induced change in catalytic rate is up to 10^5 higher than the rate of O^{2-} supply to the catalyst. These phenomena are observed when the rate is controlled by the reaction of ethylene with chemisorbed oxygen. When oxy-

gen adsorption is rate limiting there is no measurable effect on the rate.

The above observations can be accounted for by considering the changes in catalyst work function resulting from the interaction of oxygen anions with the catalyst surface. For porous metal films deposited on flat zirconia components, such as the ones used in the present investigation, a change ΔV_{WR} in catalyst potential results in a change $e\Delta V_{WR}$ in catalyst work function. The observed galvanostatic transient time constants (Table 1) together with some recent spectroscopic investigations (*43*) show that oxygen anion (most likely O^-) spillover must be occurring over the entire catalyst surface. Further surface spectroscopic investigation could lead to a better understanding of the NEMCA effect, which is of considerable theoretical and practical importance.

ACKNOWLEDGMENTS

Financial support from the VW Stiftung of the Federal Republic of Germany and from the European Economic Community Nonnuclear Energy Program is gratefully acknowledged. We also thank Professors L. Riekert and X. E. Verykios for helpful discussions and Ms. B. Georgali for the scanning electron micrographs.

REFERENCES

1. Lain, Y., Criodo, J., and Boudart, M., *Nouv. J. Chim.* **1,** 461 (1977).
2. Sachtler, J. W. A., and Somorjai, G. A., *J. Catal.* **81,** 77 (1983).
3. Ponec, V., "Advances in Catalysis" (D. D. Eley, P. W. Selwood, and Paul B. Weisz, Eds.), Vol. 32, p. 1. Academic Press, New York, 1983.
4. Imelik, B., *et al.*, "Metal–Support and Metal–Additives Effects in Catalysis." Studies in Surface Science and Catalysis, Vol. 11. Elsevier, Amsterdam, 1982.
5. Hegedus, L. L., *et al.*, "Catalyst Design: Progress and Perspectives." Wiley, New York, 1987.
6. Akubuiro, E. C., and Verykios, X. E., *J. Catal.* **103,** 320 (1987).
7. Vayenas, C. G., *Solid State Ionics* **28–30,** 1521 (1988).
8. Stoukides, M., and Vayenas, C. G., *J. Catal.* **69,** 18 (1981).
9. Stoukides, M., and Vayenas, C. G., *J. Catal.* **74,** 266 (1982).
10. Stoukides, M., and Vayenas, C. G., *J. Catal.* **82,** 45 (1983).
11. Häfele, E., and Lintz, H.-G., *Ber. BunsenGes. Phys. Chem.* **90,** 288 (1986).
12. Vayenas, C. G., Lee, B., and Michaels, J. N., *J. Catal.* **66,** 36 (1980).
13. Stoukides, M., Seimanides, S., and Vayenas, C. G., *ACS Symp. Ser.* **196,** 195 (1982).
14. Yentekakis, I. V., Neophytides, S., and Vayenas, C. G., *J. Catal.* **111,** 152 (1988).
15. Vayenas, C. G., and Farr, R. D., *Science* **208,** 593 (1980).
16. Farr, R. D., and Vayenas, C. G., *J. Electrochem. Soc.* **127,** 1478 (1980).
17. Sigal, C., and Vayenas, C. G., *Solid State Ionics* **5,** 567 (1981).
18. Michaels, J. N., and Vayenas, C. G., *J. Catal.* **85,** 477 (1984).
19. Michaels, J. N., and Vayenas, C. G., *J. Electrochem. Soc.* **131,** 2544 (1984).
20. Kiratzis, N., and Stoukides, M., *J. Electrochem. Soc.* **134,** 1925 (1987).
21. Yentekakis, I. V., and Vayenas, C. G., *J. Electrochem. Soc.* **136,** 996 (1989).
22. Vayenas, C. G., Yentekakis, I. V., and Neophytides, S., Paper 168 e, AICHE Annual Meeting, 1988.
23. Pancharatnam, S., Huggins, R. A., and Mason, D. M., *J. Electrochem. Soc.* **122,** 869 (1975).
24. Gür, T. M., and Huggins, R. A., *J. Electrochem. Soc.* **126,** 1067 (1979).
25. Gür, T. M., and Huggins, R. A., *Science* **219,** 967 (1983).
26. Gür, T. M., and Huggins, R. A., *J. Catal.* **102,** 443 (1986).
27. Stoukides, M., and Vayenas, C. G., *J. Catal.* **70,** 137 (1981).
28. Stoukides, M., and Vayenas, C. G., *ACS Symp. Ser.* **178,** 181 (1982).
29. Stoukides, M., and Vayenas, C. G., *J. Electrochem. Soc.* **131,** 839 (1984).
30. Yentekakis, I. V., and Vayenas, C. G., *J. Catal.* **111,** 170 (1988).
31. Berlowitz, P., Megiris, C., Butt, J. B., and Kung, H. H., *Langmuir* **1,** 206 (1985).
32. Kaul, D. J., and Wolf, E. E., *Chem. Eng. Sci.* **42,** 1399 (1987).
33. Palmer, R. L., *J. Vac. Sci. Technol.* **12,** 1403 (1975).
34. Steininger, H., Ibach, H., and Lehwald, S., *Surf. Sci.* **117,** 685 (1982).
35. Vayenas, C. G., Georgakis, C., Michaels, J. N., and Tormo, J., *J. Catal.* **67,** 348 (1981).
36. Neophytides, S., and Vayenas, C. G., *J. Catal.*, in press.
37. Vayenas, C. G., Bebelis, S., and Neophytides, S., *J. Phys. Chem.* **92,** 5083 (1988).

38. Vayenas, C. G., Bebelis, S., Neophytides, S., and Yentekakis, I. V., *Appl. Phys.* (*A*), in press (1989).
39. Bebelis, S., and Vayenas, C. G., in preparation.
40. Tsiakaras, P., and Vayenas, C. G., in preparation.
41. Manton, M., Ph.D. thesis, Massachusetts Institute of Technology, 1986.
42. Gundry, P. M., and Tompkins, F. C., *in* "Experimental Methods in Catalytic Research" (R. B. Anderson, Ed.), pp. 100–168. Academic Press, New York, 1968.
43. Arakawa, T., Saito, A., and Shiokawa, J., *Appl. Surf. Sci.* **16,** 365 (1983).
44. Eiswirth, M., Schwankner, R., and Ertl, G., *Z. Phys. Chem. Neue Folge* **144,** 59 (1985).
45. Wang, D. Y., and Nowick, A. S., *J. Electrochem. Soc.* **123,** 55 (1981).
46. Wang, D. Y., and Nowick, A. S., *J. Electrochem. Soc.* **126,** 1155 (1979).
47. Boudart, M., *J. Amer. Chem. Soc.* **74,** 3556 (1952).